



# Development of catalytically active and highly stable catalyst supports for polymer electrolyte membrane fuel cells



Taekeun Kim, Tianyuan Xie, Wonsuk Jung, Francis Gadala-Maria, Prabhu Ganesan, Branko N. Popov\*

Center for Electrochemical Engineering, Department of Chemical Engineering, University of South Carolina, Columbia, SC 29208, USA

## HIGHLIGHTS

- Development of highly stable and active cathode catalyst supports is reported.
- Pt nanoparticles deposited on the stable supports show enhanced catalytic activity.
- Potential holding at 1.2 V showed enhanced support stability in H<sub>2</sub>-air polarization.
- Rated power densities of 0.18–0.23 g<sub>Pt</sub> kW<sup>−1</sup> are achieved with the novel catalysts.

## ARTICLE INFO

### Article history:

Received 8 July 2014

Received in revised form

4 September 2014

Accepted 22 September 2014

Available online 2 October 2014

### Keywords:

Polymer electrolyte membrane fuel cells

Support stability

Catalyst performance

Potential holding

Electrochemical surface area

## ABSTRACT

Novel procedures are developed for the synthesis of highly stable carbon composite catalyst supports (CCCS-800 °C and CCCS-1100 °C) and an activated carbon composite catalyst support (A-CCCS). These supports are synthesized through: (i) surface modification with acids and inclusion of oxygen groups, (ii) metal-catalyzed pyrolysis, and (iii) chemical leaching to remove excess metal used to dope the support. The procedure results in increasing carbon graphitization and inclusion of non-metallic active sites on the support surface. Catalytic activity of CCCS indicates an onset potential of 0.86 V for the oxygen reduction reaction (ORR) with well-defined kinetic and mass-transfer regions and ~2.5% H<sub>2</sub>O<sub>2</sub> production in rotating ring disk electrode (RRDE) studies. Support stability studies at 1.2 V constant potential holding for 400 h indicate high stability for the 30% Pt/A-CCCS catalyst with a cell potential loss of 27 mV at 800 mA cm<sup>−2</sup> under H<sub>2</sub>-air, 32% mass activity loss, and 30% ECSA loss. Performance evaluation in polymer electrolyte membrane (PEM) fuel cell shows power densities (rated) of 0.18 and 0.23 g<sub>Pt</sub> kW<sup>−1</sup> for the 30% Pt/A-CCCS and 30% Pt/CCCS-800 °C catalysts, respectively. The stabilities of various supports developed in this study are compared with those of a commercial Pt/C catalyst.

© 2014 Elsevier B.V. All rights reserved.

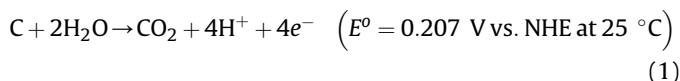
## 1. Introduction

Polymer electrolyte membrane (PEM) fuel cells have attracted attention for stationary and automotive applications due to their high efficiency, high current density output, low-temperature operation, and low emissions [1–5]. Carbon black is a typical catalyst support material for fuel cell applications because of its high electrical conductivity, large surface area, and well-defined pore structure. Platinum and Pt-based alloy catalysts supported on high surface area carbons have been used for oxygen reduction reaction (ORR) in PEM fuel cells [3,5–7]. Recent research on PEM fuel cell development mainly focuses on the reliability of the

system and durability of the catalysts and catalyst supports. The performance degradation of PEM fuel cells is affected by several factors including platinum and/or alloying element dissolution [8,9], Pt particle sintering [8–10], carbon support corrosion [11–15], and membrane thinning [8,9].

It has been reported that automotive fuel cell systems can experience excursions to very high potential regions due to repetitive shutdown/startup of the fuel cell system or due to local fuel cell starvation [16]. Reiser et al. [17] have shown that the cathode interfacial potential difference can reach ~1.5 V due to the H<sub>2</sub>/air front in the anode compartment during shutdown/startup and carbon corrosion is an inevitable parasitic reaction at these high potentials. This high potential with other favorable conditions such as the presence of Pt, low pH, high oxygen and water contents, and high temperature accelerate the carbon corrosion according to the following reaction:

\* Corresponding author. Tel.: +1 (803) 777 7314; fax: +1 (803) 777 8265.  
E-mail address: [popov@cec.sc.edu](mailto:popov@cec.sc.edu) (B.N. Popov).



In general, carbon corrosion occurs through the formation of oxygen-containing functional groups such as carboxyl, carbonyl, hydroxyl, phenol, etc. on the surface at high potentials and temperature ( $>1.0$  V vs. reversible hydrogen electrode (RHE) at room temperature or  $>0.8$  V vs. RHE at  $65^\circ\text{C}$ ) [12,13]. Fig. 1 shows a schematic of the effects of carbon corrosion on a PEM fuel cell cathode [11]. Carbon corrosion weakens the catalyst interaction with the support resulting in formation of electrically isolated Pt particles that are detached from the carbon support. Electrochemical oxidation of the carbon support results in carbon support loss which leads to Pt agglomeration and sintering and subsequent loss of electrochemical surface area (ECSA) [10,14,15]. Carbon support oxidation can increase the hydrophilicity of the surface which results in a decrease in gas permeability [18] as the pores are filled with water that hinders gas transport [19]. Carbon support loss also causes a decrease in catalyst layer thickness which increases the cell resistance [20] due to poor electrical contact with the gas diffusion layer [21,22]. Thus, carbon corrosion is a detrimental factor which affects the cathode catalyst degradation and overall PEM fuel cell performance loss.

In order to overcome the problems associated with carbon supports, alternative materials such as metal oxides [11,23–26], conducting polymers [27], non-conducting polymers [28,29], metal nitrides and metal carbides [30,31],  $\text{ZrO}_2/\text{C}$  [32,33],  $\text{CeO}_2/\text{C}$  [34] have been explored as catalyst supports for PEM fuel cell application with limited success in terms of achieving desired power density requirements necessary for automotive applications. Hence, high surface area carbons and graphitic carbons are being used as the catalyst support for PEM fuel cell applications.

Carbon corrosion in PEM fuel cell cathode catalysts has been extensively studied both in three-electrode set-up using a rotating ring disk electrode (RRDE) [35–43] and under fuel cell operating conditions [16,44–57]. Mechanistic studies to understand carbon corrosion under PEM fuel cell operating conditions have also been reported [58,59].

The effect of corrosion of BP-2000 and XC-72 carbon supports on the durability of Pt/C catalyst was studied by Wang et al. [36] by applying a constant potential of 1.2 V under simulated PEM fuel cell conditions. A larger increase in Pt particle size and a higher loss of Pt was observed in the Pt/BP-2000 catalyst than in Pt/XC-72 under potential cycling condition between 0.6 and 1.2 V. ECSA loss of 40.9% for the Pt/BP-2000 and 20.6% for the Pt/XC-72 catalysts have

been reported. Studies of the corrosion mechanism of Pt/XC-72 and Pt/BP-2000 catalysts using RRDE and observations using a transmission electron microscope indicated that major corrosion occurred inside the catalyst with some minor corrosion on the surface in the case of Pt/XC-72, whereas corrosion predominantly occurred at the surface for Pt/BP-2000 [37].

The microstructure effects on the electrochemical corrosion of furnace blacks, proprietary carbons of the Sibunit family, carbon nanofilaments, and carbon-supported Pt catalysts have been studied in a three-electrode cell in 2 M  $\text{H}_2\text{SO}_4$  at  $80^\circ\text{C}$  [38]. Corrosion currents were found to decay with time roughly following the  $t^{-0.5}$  dependence. Corrosion current densities (normalized to the surface area) depended strongly on the microstructure of the carbon material. The proprietary Sibunit carbon and carbon nanofiber possess higher corrosion stability than conventional furnace blacks. The electrochemical stability of carbon nanofiber [39], mesoporous carbon [40], nitrogen-doped reduced graphene oxide [41], and graphene oxide [42,43] supports in RRDE has also been reported. The experiments on carbon nanofibers showed that the relative increase in surface oxides during the electrochemical oxidation treatment is significantly smaller than on carbon black [39]. Potential cycling between 0.8 and 1.4 V in an RRDE indicated better stability for catalysts on Vulcan carbon due to the presence of larger average graphitic crystallites than for catalysts supported on high-surface-area ordered mesoporous carbon. [40]. Graphene oxide (GO) has been used as a support for the cathode catalyst in PEM fuel cells because its oxygen-containing groups act as binding sites for Pt nanoparticles [41–43]. Unlike conventional Pt catalysts, a Pt catalyst supported on nitrogen-doped reduced graphene oxide showed no performance degradation after 1000 cycles between 0.6 and 1.2 V in an accelerated durability test (ADT) [41]. He et al. [42] suggested a bifunctional effect of both graphitization and oxygen functional groups on the catalytic activity and stabilization of Pt nanoparticles deposited on reduced graphene oxide (Pt/RGO) catalysts. The support durability test results using three-electrode cell studies offer only limited information about the stability of various carbon supports and do not provide any insight into the durability of these supports in PEM fuel cells under actual startup/shutdown conditions.

The support durability of various carbon-supported Pt catalysts subjected to different accelerated corrosion tests in PEM fuel cells has been reported in the literature [16,44–58]. Wang et al. [44] carried out support corrosion characterization studies on multi-wall carbon nanotube (MWCNT) and commercial Vulcan XC-72 supports using potentiostatic treatment (0.9 V) for 168 h. They

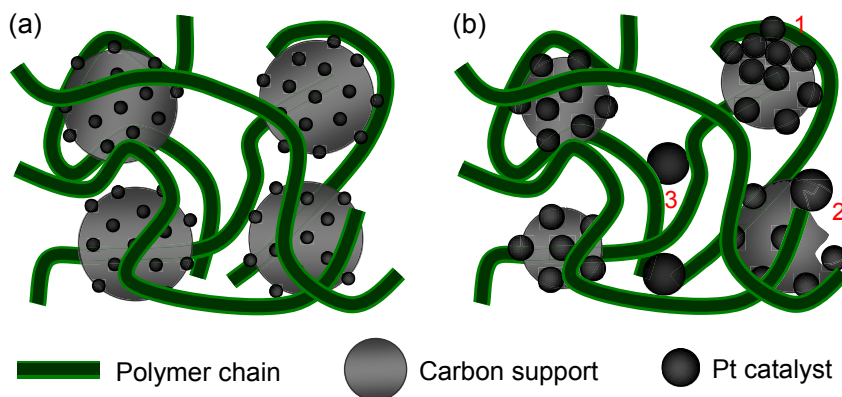


**Fig. 1.** Schematic representation of the effect of carbon corrosion on (1) agglomeration, (2) coalescence, and (3) loss of Pt particles in the MEA during operation of PEM fuel cells: (a) normal (corrosion-resistant) electrode and (b) corroded electrode [11]. "Reprinted (adapted) with permission from Sheng-Yang Huang, Prabhu Ganesan, Sehkyu Park, and Branko N. Popov, J. Am. Chem. Soc., 131 (2009) 13898–13899. Copyright© 2009 Journal of American Chemical Society."

concluded that the multiwall carbon nanotube support is electrochemically more stable than the Vulcan XC-72 support since the former showed 30% lower corrosion current and a 37% loss in ECSA (80% loss in ECSA for Vulcan XC-72) after applying a constant potential of 0.9 V for 168 h. However, the experimental conditions used in this study do not effectively induce carbon corrosion since the extent of carbon corrosion is significant only at potentials >1.0 V. Bi and Fuller [45] studied the effect of temperature on carbon corrosion in Pt/C under accelerated conditions by applying a square-wave potential cycling between 0.87 and 1.2 V vs. RHE. More rapid degradation was observed due to loss of ECSA and Pt deposition on the membrane at 80 °C than at 60 or 40 °C.

Oh et al. [46,47] and Lim et al. [48,49] studied carbon corrosion in a variety of carbons such as carbon black (CB), carbon nanofiber (CNF) and carbon nanocage (CNC) in Pt/CB, Pt/CNF and Pt/CNC catalysts by applying a constant potential of 1.4 V for 30 min. Using on-line mass spectrometry, they measured the amount of CO<sub>2</sub> produced when these catalysts were subjected to a high potential. A comparison study involving Pt/CB, Pt/CNF and Pt/CNC by Oh et al. [46] indicated that the degree of graphitization did not directly correlate to the higher corrosion resistance. The authors concluded that hydrophobicity was a critical factor in enhancing the supports' resistance to corrosion and that carbon nanocage was more resistant to corrosion than carbon nanofiber. Lim et al. [48] also found significant corrosion resistance for the carbon nanocage support with 2.3% performance degradation at 0.6 V under H<sub>2</sub>/O<sub>2</sub> fuel cell polarization after applying 1.4 V to the cathode for 30 min. In a separate study, Lim et al. [49] showed that the presence of water is indispensable for and the presence of gas-phase O<sub>2</sub> has little effect on the electrochemical carbon corrosion.

The durability of graphitic carbon (GrC) [50,51] and graphitized MWCNT [52] supports was studied through accelerated stress tests (AST) using potentiostatic (potential holding at 1.2 V) [50,52] and potential cycling (between 0.6 and 1.2 V) [51] experiments. Application of the constant potential to the Pt/GrC and Pt/non-GrC cathodes showed fuel cell performance degradation of only 10% after 70 h for the Pt/GrC and a much higher loss (77%) for the Pt/non-GrC [50] in a H<sub>2</sub>–O<sub>2</sub> fuel cell. The AST study for Pt<sub>3</sub>Co and Pt catalysts supported on graphitic and non-graphitic carbon supports subjected to potential cycling between 0.6 and 1.2 V indicated an order of durability of Pt<sub>3</sub>Co/GrC > Pt/GrC > Pt<sub>3</sub>Co/non-GrC > Pt/non-GrC [51]. The comparison study involving Pt/C, pristine, and graphitized Pt/MWCNT catalysts showed Pt particle growth in the Pt/C catalyst after subjecting it to AST at 1.2 V [52]. The study concluded that Pt particles have a high tendency to aggregate upon carbon corrosion during AST because of their high surface-energy. Furthermore, in Pt/C, the amorphous nature of carbon with a higher number of defect sites facilitates carbon corrosion resulting in larger particles relative to Pt deposited on pristine and graphitized MWCNTs [52].

A simple low-temperature self-catalyzed reduction treatment has been shown to improve the support durability at 1.4 V of the carbon nanotube (CNT) supports. Studies consisting of an accelerated test for 6 h followed by electrochemical characterization studies including ECSA measurement and H<sub>2</sub>–O<sub>2</sub> polarization curve indicated an activity loss of 62.5% for the commercial Pt/C and of only 6.2% for the CNT subjected to self-catalyzed reduction treatment. An increase in polarization resistance of 3% for the Pt/CNT as opposed to a 700% increase for the Pt/C has been reported [53].

Dhanushkodi et al. [54] used a variety of voltage waveforms such as two square wave potential cycling (from 1.0 V to 1.4 V and from 1.0 V to 1.5 V) with different dwell times and constant cell voltage of 1.4 V to elucidate the extent of carbon corrosion, mixed-mode degradation, and Pt dissolution.

The durability of Pt/C and of Pt deposited on mesoporous carbon functionalized with poly(3,4-ethylenedioxythiophene) (MC-PEDOT) has been reported by Tintula et al. [55]. They found the degradation rate for Pt/C in a H<sub>2</sub>–O<sub>2</sub> fuel cell is three times higher than that for Pt/MC-PEDOT. The authors concluded that the enhanced durability of Pt/MC-PEDOT is due to the specific interaction of Pt with the MC-PEDOT support and the resistance toward electrochemical oxidation of the mesoporous carbon support.

Other studies of importance with respect to the carbon support corrosion were reported by Makharia et al. [16], Jung et al. [56], and Spornjak et al. [57]. Makharia et al. [16], after studying the support stability by calculating the mass-specific CO<sub>2</sub> currents by online gas analysis as a function of potential (1.1–1.3 V vs. RHE), temperature (50–95 °C), and time (1000 min), suggested that future R&D efforts should focus on the development of more stable catalyst supports with improved corrosion resistance at high cathodic potentials. Carbon corrosion in 50% Pt/C and 30% Pt-alloy/corrosion-resistant carbon catalysts were evaluated by recording H<sub>2</sub>–air polarization curves using a stoic of 3/3 at 80 °C with 50% relative humidity (RH) and 150 kPa<sub>abs</sub> back pressure. Their study showed that after 20 h of potentiostatic holding at 1.2 V, the H<sub>2</sub>–air performance of a Pt/C catalyst decreases 30 mV at 1500 mA cm<sup>−2</sup> and much more after 30 h, while the 30% Pt-alloy/corrosion-resistant support showed no decrease in performance even after 100 h of exposure at 1.2 V. A correlation between voltage loss and carbon-support weight loss indicated that both conventional and corrosion-resistant support electrode structures show high performance losses at about 5–10% carbon-support weight loss.

However, to the best of our knowledge, very limited reports are available on the potential loss under H<sub>2</sub>–air polarization performance after subjecting the cathode catalysts to constant potentials to induce carbon corrosion. These studies are important for the development of corrosion-resistant carbon supports for automotive applications since the fuel cell stack can spend a significant period of its operating time at open circuit voltage (OCV) at the operating temperature (80 °C) totaling a few hundred hours during startup/shutdown cycles [16]. Other reported results primarily compare the performance degradation in H<sub>2</sub>–O<sub>2</sub> polarization [42–50] as opposed to a more practical H<sub>2</sub>–air polarization which is necessary for the development of stable catalysts and supports for PEM fuel cells to be used for automotive applications. Therefore, the overall objectives of the present study are to develop catalytically active and highly stable cathode catalyst supports and to study their stability using a potential holding experiment (1.2 V for 400 h) by comparing the potential loss at 800 mA cm<sup>−2</sup> under H<sub>2</sub>–air fuel cell operating conditions.

The specific objectives are:

- (i) To develop carbon composite catalyst supports (CCCS) and an activated carbon composite catalyst support (A-CCCS) having desired BET surface area and pore-size distribution with well-defined kinetic and mass transfer regions during the oxygen reduction reaction.
- (ii) To modify the surface of CCCS and A-CCCS to facilitate uniform platinum deposition.
- (iii) To study the ORR activity for CCCS and synergistic activity of Pt/CCCS in a three-electrode cell using RRDE and evaluate of the performance for the Pt/CCCS and Pt/A-CCCS catalysts in PEM fuel cells with 25 cm<sup>2</sup> membrane electrode assemblies (MEAs).
- (iv) To evaluate the support stability for Pt/CCCS and Pt/A-CCCS catalysts under potentiostatic conditions (applying 1.2 V to the cathode for 400 h) by measuring the cell potential loss at 800 mA cm<sup>−2</sup> and to compare the results with the stability of

commercial Pt/C catalyst deposited on high surface area carbon.

In this study, we present the catalytic activity of CCCS towards ORR and the synergistic effect that exists between the CCCS and Pt active sites in a Pt/CCCS catalyst. Three Pt catalysts, namely Pt/CCCS-800 °C, Pt/CCCS-1100 °C, and Pt/A-CCCS, were synthesized using two CCCS (abbreviated as CCCS-800 °C and CCCS-1100 °C) and one activated CCCS (abbreviated as A-CCCS). The results obtained for initial H<sub>2</sub>–O<sub>2</sub> and H<sub>2</sub>–air fuel cell performance and support stability are compared with those of commercial Pt/C catalyst deposited on high surface area carbon.

## 2. Experimental

### 2.1. Development of carbon composite catalyst supports (CCCS) and an activated carbon composite catalyst support (A-CCCS)

A methodology for highly active carbon composite catalysts has been developed at University of South Carolina and reported in our previous studies [5,60–67]. The CCCS was synthesized from Ketjen black (EC 300J). In brief, the as-received Ketjen black was refluxed in a concentrated HNO<sub>3</sub> solution at 80 °C to introduce oxygen functional groups into the carbon surface. Then, the oxidized carbons were subjected to a metal-catalyzed pyrolysis process in the presence of variety of transition metals, such as Co and Fe, and nitrogen-containing organic compounds to introduce pyridinic-nitrogen active sites followed by pyrolysis at different temperatures. Then, the resulting product was leached in 0.5 M H<sub>2</sub>SO<sub>4</sub> to remove excess metals from the pyrolysis and graphitization process. Four types of CCCS were synthesized using heat treatment temperatures of 800 °C (CCCS-800 °C), 1100 °C (CCCS-1100 °C), 1300 °C (CCCS-1300 °C), and 1500 °C (CCCS-1500 °C). The A-CCCS was synthesized by heat treating a carbon source at 800 °C in the presence of only nitrogen-containing compound (no transition metals were used) followed by purification and stabilization processes to remove the electrochemically unstable carbon from the final product.

### 2.2. Surface modification and platinum deposition

A surface functionalization process to increase the hydrophilic property of CCCS and A-CCCS was developed using a bifunctional organic molecule containing aromatic hydrocarbon and acid groups. A surface modification process is necessary in order to obtain a uniform Pt particle size distribution on the CCCS. Ketjen black and CCCS-800 °C were used for the synthesis of 5% Pt/C and 5% Pt/CCCS-800 °C catalysts, respectively. Platinum nanoparticle deposition with an initial loading of 5 and 30 wt% Pt was carried out using a modified polyol process, which uses additives to control the particle size and enhance the catalyst–support interaction. In brief, a measured amount of PtCl<sub>4</sub> was dissolved in an appropriate volume of ethylene glycol under vigorous stirring for 30 min. 0.1 M NaOH was introduced into the solution to adjust the pH. The pH of the reaction mixture was precisely controlled at every step of the process in order to obtain a uniform Pt deposition. Then, calculated amounts of CCCS or A-CCCS were added to the solution so that the desired initial Pt loading was achieved in the final Pt/CCCS and Pt/A-CCCS catalysts. The resulting suspension was stirred for 1 h at room temperature followed by refluxing at 160 °C for 3 h. The solution was allowed to cool down to room temperature and kept for 12 h under continuous stirring. 0.1 M H<sub>2</sub>SO<sub>4</sub> was then added to the cooled mixture and the solution pH was adjusted to 3. The mixture was kept stirred for 24 h. The Pt/CCCS and Pt/A-CCCS catalysts in the solution were filtered and thoroughly washed with de-ionized

water. The resulting carbon-supported Pt catalysts were dried in air for 1 h at 160 °C and stored for further studies.

### 2.3. Material characterization studies

The physical properties of CCCS and A-CCCS and Pt/CCCS and Pt/A-CCCS catalysts were studied using a variety of physical characterization techniques such as X-ray diffraction (XRD), Brunauer–Emmett–Teller (BET) surface area analysis, X-ray fluorescence (XRF), inductively coupled plasma-atomic emission spectroscopy (ICP-AES) analysis, and high resolution transmission electron microscopy (HRTEM). XRD patterns were recorded using Rigaku 405S5 to identify the crystalline structure of the synthesized supports and catalysts. Raman spectroscopy (HORIBA “LABRAM 1B” with He–Ne 20 mW laser, wave length 632.817 nm) was used to evaluate the degree of graphitization of the carbon supports. BET (Quantachrome) was used to determine the surface area and pore-size distribution of the CCCS and A-CCCS. XRF was used to confirm the Pt loading on the cathode and anode electrodes. HRTEM (Hitachi H9500) was used to determine the particle size and particle size distribution of Pt/CCCS and Pt/A-CCCS catalysts. ICP-AES (Perkin Elmer) analysis was used to determine the composition CCCS and A-CCCS and Pt/CCCS and Pt/A-CCCS catalysts.

### 2.4. Electrochemical characterization studies

Electrochemical RRDE characterization studies were performed in 0.1 M HClO<sub>4</sub> using a Pine bipotentiostat (Model AFCBP1), a Pt-mesh counter electrode, and an Ag/AgCl reference electrode (0.254 V vs. RHE). RRDE with a Pt-ring and a glassy carbon disk (0.247 cm<sup>2</sup>) was used as the working electrode. The catalyst ink was prepared by blending the catalyst powder (CCCS, A-CCCS, Pt/CCCS or Pt/A-CCCS) with a 5% solution of Nafion<sup>®</sup> and isopropanol in an ultrasonic bath. The synergistic effect of CCCS and Pt catalyst was studied by comparing the ORR activities of 5% Pt deposited on CCCS-800 °C and on Ketjen black. The 30 wt% Pt catalysts were used for comparing the ORR activities of Pt/CCCS and Pt/A-CCCS catalysts. Appropriate quantities of the catalyst inks were deposited on the glassy carbon disk using a micropipette to achieve loadings of 20 μg<sub>Pt</sub> cm<sup>−2</sup> for Pt/C, Pt/CCCS, and Pt/A-CCCS catalysts and 100 μg cm<sup>−2</sup> for Ketjen Black, CCCS, and A-CCCS, respectively. ECSA of the Pt catalysts was determined by charge integration under the hydrogen desorption peaks appearing between 0 and 0.35 V, by assuming a charge of 210 μC cm<sup>−2</sup> for the electroactive Pt surface [68]. The specific ECSA was calculated based on the following equation:

$$\text{Specific ECSA} = \frac{Q_H}{m \times q_H} \quad (2)$$

where  $Q_H$  is the charge for hydrogen desorption,  $m$  is the Pt metal loading, and  $q_H$  is the charge required for desorbing a monolayer of hydrogen on Pt surface. After the ECSA measurements, the electrolyte was purged with oxygen for 30 min prior to the oxygen reduction reaction kinetics measurement using linear sweep voltammetry (LSV) at a scan rate of 5 mV s<sup>−1</sup>. The oxygen reduction current was calculated from the difference between currents measured in the nitrogen- and oxygen-saturated electrolytes.

### 2.5. Fuel cell performance and stability studies

The polarization performances of Pt/C, Pt/CCCS and Pt/A-CCCS catalysts were evaluated in 25 cm<sup>2</sup> MEAs using commercial Pt/C (46.7% Pt/C obtained from Tanaka Kikinzoku Kogyo (TKK) corporation, Japan) as the anode. The catalyst inks for the anode and cathode were prepared by blending the catalysts (Pt/C, Pt/CCCS or

Pt/A-CCCS) in a 5% solution of Nafion® in isopropyl alcohol (Alfa Aesar) in an ultrasonic bath. Commercially available carbon paper (SGL 10 BC) was used as the gas diffusion media for the anode preparation. The cathode catalysts were directly deposited onto the Nafion® NRE 212 membrane. The anode and cathode catalyst loading was fixed at  $0.1 \text{ mg}_{\text{Pt}} \text{ cm}^{-2}$  and confirmed using XRF. The catalyst-coated anode electrode was hot-pressed onto the blank side of the cathode-catalyst coated Nafion® membrane at  $140^\circ\text{C}$  for 3 min under 200 psi to form the MEAs. A blank SGL 10 BC carbon paper was used as the gas diffusion media on the cathode side. Initially, the MEA was activated under a supply of  $\text{H}_2$  and  $\text{O}_2$  at  $80^\circ\text{C}$  to the anode and cathode compartments, respectively, and the initial polarization performance curves were recorded with a flow rate of  $750 \text{ ml min}^{-1}$  and 100% RH.

The support stability was evaluated using a potentiostatic experiment. The potential holding experiment was performed by applying 1.2 V constant potential to the cathode with respect to the anode for 400 h at a cell temperature of  $80^\circ\text{C}$ . During the experiment, pure hydrogen ( $200 \text{ cc min}^{-1}$ ) and nitrogen ( $75 \text{ cc min}^{-1}$ )

having 100% RH were supplied to the anode and cathode compartments under  $150 \text{ kPa}_{\text{abs}}$  back pressure, respectively. The catalyst mass activity was evaluated under  $\text{H}_2/\text{O}_2$  (2/9.5 stoic.) at  $80^\circ\text{C}$ , 100% RH, and  $150 \text{ kPa}_{\text{abs}}$  back pressure. The polarization curves were recorded under  $\text{H}_2/\text{air}$  (2/2 stoic.) at  $80^\circ\text{C}$ , 50% RH, and  $170 \text{ kPa}_{\text{abs}}$  back pressure. The loss in catalyst mass activity and the potential loss under  $\text{H}_2/\text{air}$  after 400 h potential holding were used to evaluate the support stability in Pt/CCCS and Pt/A-CCCS catalysts.

### 3. Results and discussions

#### 3.1. Development of carbon composite catalyst supports (CCCS) and an activated carbon composite catalyst support (A-CCCS)

The XRD patterns of CCCS synthesized at heat treatment temperatures between  $800$  and  $1500^\circ\text{C}$  and of A-CCCS are shown in Fig. 2(a) and (b), respectively. In the case of CCCS, the degree of graphitization increases with pyrolysis temperature. The crystallite thickness ( $L_c$ ) calculated by Scherrer's formula and the interlayer spacing ( $d_{002}$ ) obtained from Bragg's law, are given in Table 1. It has been reported that higher  $L_c$  values of the (002) peak and lower  $d_{002}$  numbers imply higher degree of graphitization [69,70]. The ratio between the D and G peaks ( $I_D/I_G$ ) obtained from Raman spectroscopy along with values for  $L_c$  and  $d_{002}$  for various CCCS are given in Table 1. For the CCCS, the  $L_c$  value increased and both  $d_{002}$  and the  $I_D/I_G$  ratio decreased as a function of pyrolysis temperature indicating the increased degree of graphitization. As shown in Fig. 2(b), the XRD did not show significant graphitic structures after the two-step process (oxidation for 1–4 h followed by pyrolysis at  $800^\circ\text{C}$  in nitrogen). The  $L_c$  and  $d_{002}$  values for the carbon source after heat treatment at  $800^\circ\text{C}$  used for the synthesis of A-CCCS are 2.8 and 0.351, respectively with an  $I_D/I_G$  ratio of 1.87. The two-step process to synthesize A-CCCS resulted in an  $L_c$  value of 2.9 and an  $I_D/I_G$  ratio of 2.48 indicating an increase in defects in the graphitic structure [42,71,72]. The increase in graphitic structure defects can be attributed to the inclusion of functional groups in the two-step process used for the synthesis of A-CCCS.

The HRTEM images shown in Fig. 3 for various CCCS also confirm the increase in degree of graphitization with the increase in heat-treatment temperatures. While the starting material, Ketjen black, is amorphous in nature, as evidenced by the XRD and HRTEM analyses, the CCCS synthesized at high temperatures show graphitic carbon tubes and carbon fiber structure formation during metal-catalyzed pyrolysis. Highly graphitized crystalline carbon structures are formed in CCCS synthesized at temperatures above  $1000^\circ\text{C}$ . The difference in surface morphology for the A-CCCS is due to the processes involved in non-metal assisted pyrolysis and the stabilization process to remove the electrochemically unstable carbon.

As shown in Table 2, BET analysis of various carbon supports indicated surface area values of 800, 400, 250, 190, 160, and  $200 \text{ m}^2 \text{ g}^{-1}$  for Ketjen black, CCCS- $800^\circ\text{C}$ , CCCS- $1100^\circ\text{C}$ , CCCS- $1300^\circ\text{C}$ , CCCS- $1500^\circ\text{C}$ , and A-CCCS, respectively. The BET surface area decreased for different CCCS as the heat treatment temperature increased due to the removal of micropores and high degree of

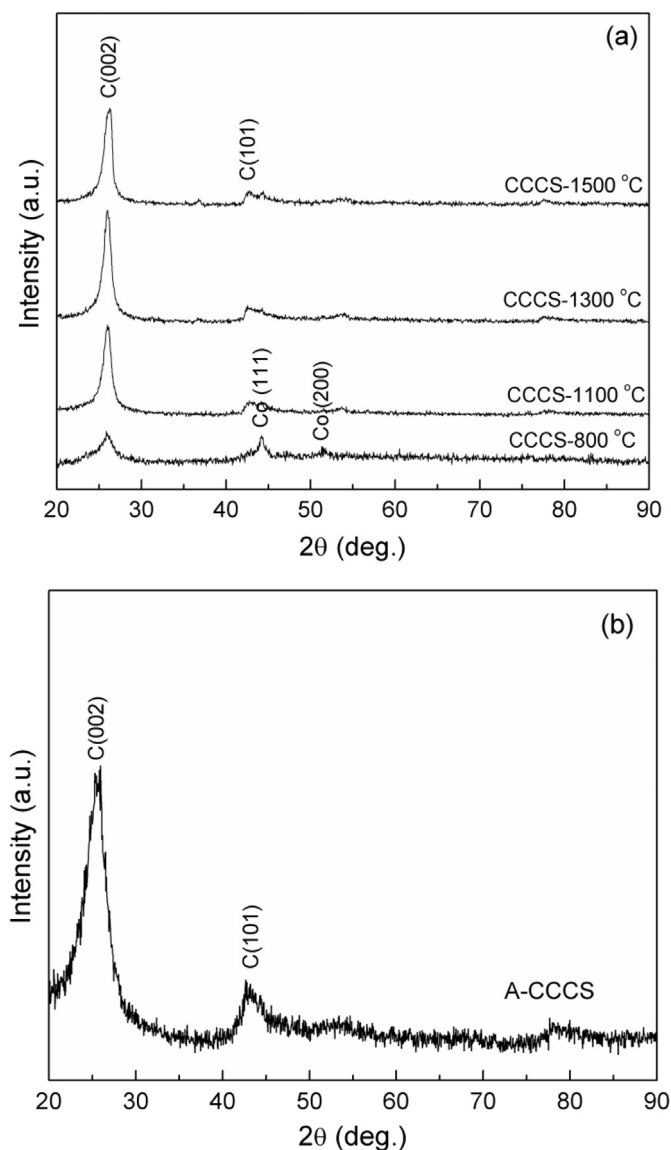
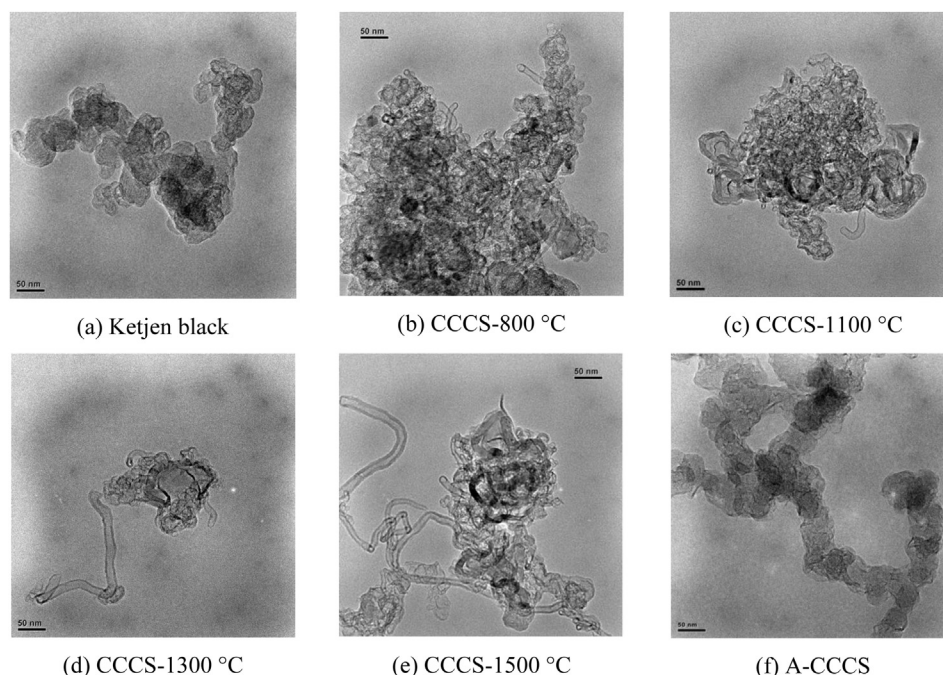


Fig. 2. X-ray diffraction patterns of CCCS and A-CCCS. (a) Comparison of CCCS synthesized at different heat treatment temperatures and Ketjen black and (b) A-CCCS.

Table 1  
The degree of graphitization for different CCCS.

Sample	Pyrolysis temperature ( $^\circ\text{C}$ )	$L_c$ (nm) (XRD)	$d_{002}$ (nm) (XRD)	$I_D/I_G$ (Raman)
Ketjen black	—	1.1	0.3613	1.60
CCCS- $800^\circ\text{C}$	800	3.6	0.3440	1.43
CCCS- $1100^\circ\text{C}$	1100	7.3	0.3431	1.25
CCCS- $1300^\circ\text{C}$	1300	7.8	0.3430	1.07
CCCS- $1500^\circ\text{C}$	1500	7.9	0.3416	0.83



**Fig. 3.** HRTEM images of (a) Ketjen black, (b) CCCS-800 °C, (c) CCCS-1100 °C, (d) CCCS-1300 °C, (e) CCCS-1500 °C, and (f) A-CCCS. The scale bar is 50 nm.

graphitization occurred at temperatures  $>1000$  °C. Of the various CCCS developed in this study, the CCCS having BET surface areas of 400 (CCCS-800 °C), 250 (CCCS-1100 °C), and  $200 \text{ m}^2 \text{ g}^{-1}$  (A-CCCS) were selected for surface modification and Pt deposition to evaluate their stability under constant potential. Commercially available Pt/C (TEC10E50E, 46.7% Pt on Ketjen Black carbon) obtained from TKK, Japan was used for the comparison studies [73].

### 3.2. Electrochemical characterization of CCCS

Comparison of ORR kinetics of Ketjen black and CCCS-800 °C and hydrogen peroxide formation on CCCS-800 °C are shown in Fig. 4(a) and (b), respectively. Ketjen black shows no activity in terms of onset potential for ORR and diffusion current when compared to CCCS-800 °C which shows onset potentials of  $\sim 0.86$  V vs. RHE and well-defined kinetic and mass-transfer regions in 0.1 M  $\text{HClO}_4$  electrolyte at room temperature. The ORR on A-CCCS exhibits similar activity as CCCS-800 °C, however without well-defined diffusion-controlled region (not shown in Fig. 4(a)).

Koutecky–Levich analysis resulted in slopes close to that for the theoretical four-electron transfer reaction with the calculated number of transferred electrons of about 3.6 for CCCS. The RRDE studies also indicated that the  $\text{H}_2\text{O}_2$  production on CCCS-800 °C is only 2.5% (Fig. 4(b)). The formation of  $\text{H}_2\text{O}_2$  is detrimental to the Nafion® membrane and the ionomer in PEM fuel cells [74]. Studies carried out by Sethuraman et al. [73] and Stamenkovic et al. [75]

correlate the %  $\text{H}_2\text{O}_2$  production to the number of electron transferred during ORR in acid electrolytes. Stamenkovic et al. [75] reported that the kinetics/reaction pathways of the oxygen reduction reaction on Pt-poly and Pt (110) are almost identical, i.e., the  $4 e^-$  reduction (with ca. 5–10% of  $\text{H}_2\text{O}_2$  production at 0.1 V) is operative on Pt-poly in acid solutions. Since the  $\text{H}_2\text{O}_2$  production is less than 5% on CCCS-800 °C, the ORR kinetics follows the  $4 e^-$  reduction pathways and is similar to that on Pt catalysts. Similar results have been reported in our previous studies for various non-precious metal catalysts [5,60–67]. Our previous studies on various non-precious metal catalysts showed that high temperature pyrolysis produces pyridinic and graphitic-type nitrogen on the surface of CCCS and the pyridinic-nitrogen groups act as catalytic sites for the oxygen reduction reaction [5,60–67]. Maldonado et al. [76] have reported that a strong Lewis basicity of such nitrogen-modified sites facilitates the reductive adsorption of oxygen without the irreversible formation of oxygen functionalities, due to an increase in the electron-donor property of carbon. The surface analysis using X-ray photoelectron spectroscopy did not show the presence of cobalt and indicated the presence of only carbon, nitrogen, and oxygen on the CCCS surface (Table 3). It is important to note that Co is present only in the bulk as indicated by the ICP-AES analysis. The Co content determined using ICP-AES indicate that the CCCS-800 °C supports have  $\sim 10$  wt% Co after 8 h leaching in 0.5 M  $\text{H}_2\text{SO}_4$  (Fig. 5). Thus, the ORR catalytic activity of CCCS is due to the presence of pyridinic-nitrogen groups and addition of Co for metal-catalyzed pyrolysis helps the inclusion of nitrogen into the CCCS [5,60–67].

### 3.3. Surface modification and Pt deposition

It is generally accepted that oxygen functional groups transform carbon surfaces from hydrophobic to hydrophilic. The hydrophilicity of as-synthesized CCCS and surface-modified CCCS is evaluated by observing dispersions of CCCS in de-ionized water. Initially, the CCCS samples are uniformly dispersed in water using an ultrasonic bath. After 1 h, the as-synthesized CCCS that did not undergo functionalization formed large aggregates and settled down

**Table 2**  
Comparison of physical properties of various CCCS, 30% Pt/CCCS catalysts, and commercial 46.7% Pt/C catalyst.

Supports	Catalysts	Pt particle size (nm)	BET surface area of the support ( $\text{m}^2 \text{ g}^{-1}$ )
Ketjen black	Commercial 46.7% Pt/C	2.0	800 [73]
CCCS-800 °C	30% Pt/CCCS-800 °C	2.2	400
CCCS-1100 °C	30% Pt/CCCS-1100 °C	2.5	250
CCCS-1300 °C	—	—	190
CCCS-1500 °C	—	—	160
A-CCCS	30% Pt/A-CCCS	3.1	200

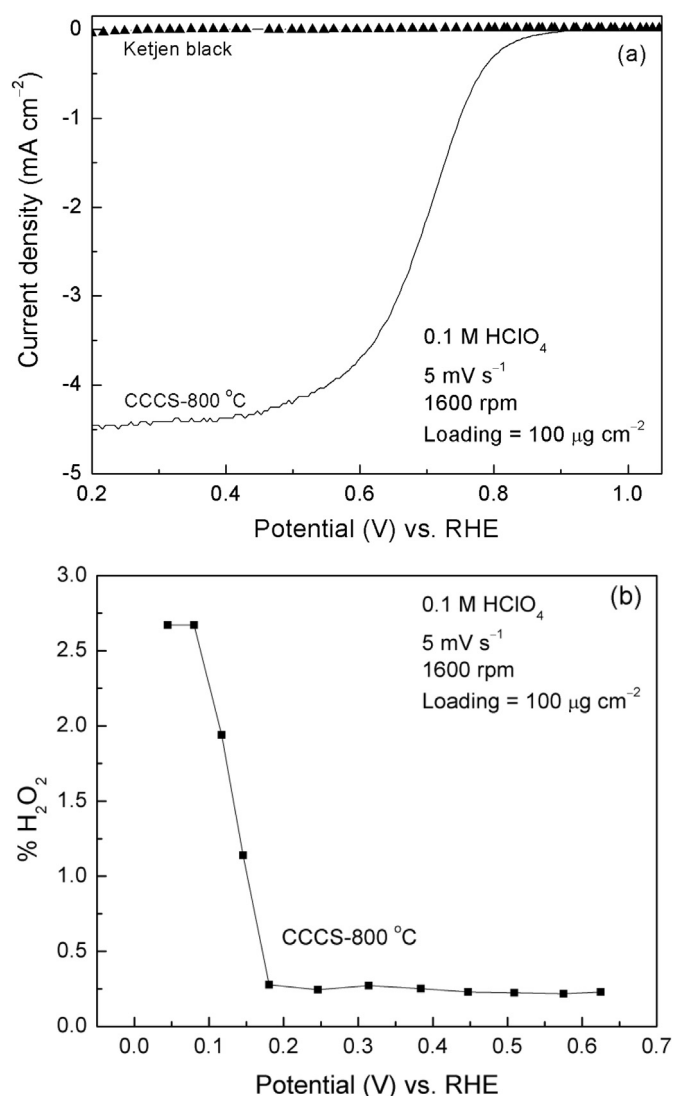


**Fig. 4.** Linear sweep voltammetry of Ketjen black and CCCS-800 °C. (a) Comparison of ORR kinetics of Ketjen black and CCCS-800 °C and (b) H<sub>2</sub>O<sub>2</sub> production on CCCS-800 °C.

completely. The functionalized CCCS remained a stable dispersion for at least 24 h in aqueous media. The stability of surface functionalized CCCS in water is attributed to the grafting of oxygen-containing groups onto the support surface which endows it with negative charges and provides the electrostatic stability required for a colloidal dispersion. Fig. 6(a–c) shows the HRTEM images of CCCS and Pt/CCCS catalysts prepared with and without surface modification. The effectiveness of surface functionalization of CCCS to obtain uniform Pt deposition is clearly shown in Fig. 6(b) whereas Fig. 6(c) shows non-uniform Pt deposition. The non-modified CCCS shows partial Pt deposition due to the hydrophobic nature of the CCCS surface. The surface-modified CCCS promotes uniform Pt deposition which is essential for achieving high catalyst utilization and durability in PEM fuel cells. In this study, 30% Pt/CCCS-800 °C, 30% Pt/CCCS-1100 °C, and 30% Pt/A-CCCS catalysts are synthesized using a modified polyol reduction process. The Pt deposition process parameters have been optimized to obtain uniform Pt deposition with an average Pt particle size,  $d_{Pt}$ , of 2–4 nm on various supports used in this study.

The XRD patterns of commercial 46.7% Pt/C, 30% Pt/CCCS-800 °C, 30% Pt/CCCS-1100 °C, and 30% Pt/A-CCCS catalysts are

compared in Fig. 7. The diffraction patterns represent all the reflections corresponding to the face centered cubic (fcc) lattice of Pt supported on various CCCS. The diffraction peak appearing at 26° for the Pt/CCCS-1100 °C and Pt/A-CCCS catalysts can be attributed to C(002) of the supports. Table 2 compares the Pt particle sizes and BET surface area of the supports used for Pt/CCCS and Pt/A-CCCS catalyst preparation. Scherrer's equation was used for calculating the Pt crystallite size using the Pt(220) peak appearing at 67.5° [18,60]. The  $d_{Pt}$  values calculated from the XRD analysis are 2.0, 2.2, 2.5, and 3.1 nm for the commercial 46.7% Pt/C, 30% Pt/CCCS-800 °C, 30% Pt/CCCS-1100 °C, and 30% Pt/A-CCCS catalysts, respectively, which are confirmed by the HRTEM and corresponding particle size distribution shown in Fig. 8.

### 3.4. Evaluation of synergistic effect

One of the objectives of this study is to combine the catalytic activity of CCCS and Pt and to show that the synergistic effect of the resulting Pt/CCCS catalyst results in enhanced ORR activity. For this purpose, 5% Pt supported catalysts are synthesized using CCCS-800 °C and Ketjen black and their ORR activities are compared. Fig. 9 shows the comparison of ORR activities of CCCS-800 °C, 5% Pt/C, and 5% Pt/CCCS-800 °C catalysts. The catalyst loadings in the glassy carbon disk are 100 μg cm<sup>-2</sup> for the CCCS-800 °C and 20 μg cm<sup>-2</sup> for the Pt/CCCS-800 °C and Pt/C catalysts. The catalyst loadings of CCCS-800 °C and Pt catalysts were chosen based on the loading effect studies which indicated mass transfer-controlled reaction kinetics for these catalysts. The onset potentials for ORR for CCCS-800 °C, 5% Pt/C, and 5% Pt/CCCS-800 °C are 0.86, 0.97, and 1.01 V, respectively. The current density values at 0.8 V (vs. RHE) for the CCCS-800 °C, 5% Pt/C, and 5% Pt/CCCS-800 °C catalysts are 0.3, 1.9, and 3.9 mA cm<sup>-2</sup>, respectively. Furthermore, the diffusion currents of CCCS-800 °C, 5% Pt/C, and 5% Pt/CCCS-800 °C catalysts are 4.5, 4.9, and 5.6 mA cm<sup>-2</sup>, respectively. For 5% Pt, with Pt loading of 20 μg cm<sup>-2</sup>, the carbon loading is 380 μg cm<sup>-2</sup>, which may result in thicker catalyst layer. Thus, the higher limiting current density,  $i_L$ , for 5% Pt/CCCS-800 °C than that for 5% Pt/C may be attributed to the difference in the catalyst layer thickness on the glassy carbon electrode according to the following equation [77]:

$$i_L = \frac{DnFC_b}{\delta} \quad (3)$$

where  $D$  is the diffusion coefficient of the reacting species,  $n$  is the number of electrons participating in the reaction,  $F$  is Faraday's constant,  $C_b$  is the concentration of the electroactive species in the bulk of the electrolyte, and  $\delta$  is the diffusion layer thickness. In the case of the 5% Pt/CCCS-800 °C catalyst, the BET surface area of the CCCS-800 °C support is much smaller (400 m<sup>2</sup> g<sup>-1</sup>) than that of the Ketjen black support (800 m<sup>2</sup> g<sup>-1</sup>) which was used to synthesize 5% Pt/C. Therefore, the 5% Pt/CCCS-800 °C catalyst shows larger limiting current density due to a much thinner catalyst layer than the 5% Pt/C catalyst. Since the experimental conditions are identical for the 5% Pt/C and 5% Pt/CCCS-800 °C catalysts, the enhanced activity as evidenced by the increase of 40 mV in the ORR onset potential and the doubling of the currents in the kinetic region can be attributed to the synergistic effect on activity of the CCCS-800 °C and Pt catalyst.

### 3.5. Performance evaluation of Pt/CCCS and Pt/A-CCCS catalysts

Fig. 10 shows the comparison of polarization curves for ORR of 30% Pt/CCCS-800 °C, 30% Pt/CCCS-1100 °C, and 30% Pt/A-CCCS catalysts at a scan rate of 5 mV s<sup>-1</sup> in 0.1 M HClO<sub>4</sub>. The shape of the voltammograms of all the catalysts shows the well-defined

**Table 3**  
XPS analysis of CCCS-800 °C.

Surface concentration determined by XPS (wt%)				
C	O	N	Co	Fe
94.86	1.26	3.88	—	—

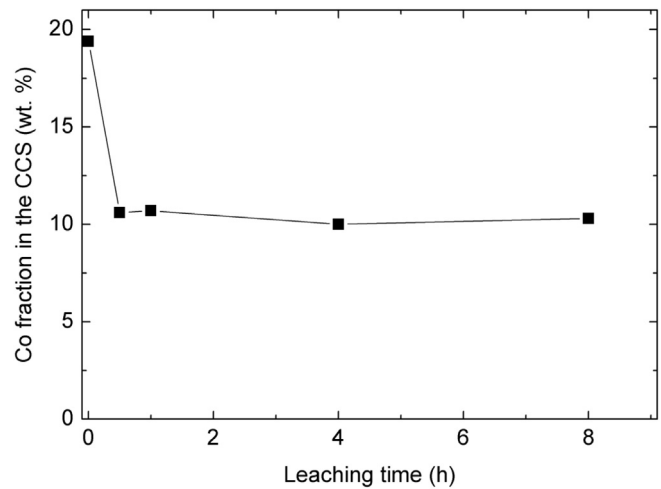


**Fig. 5.** Effect of leaching time on the Co content in CCCS-800 °C support determined by ICP-AES.

kinetic and mass transfer regions which are typical of Pt-based catalysts. The ORR is under mixed kinetic-diffusion control in the potential region between 0.95 V and 0.60 V, followed by the region where the diffusion limiting currents are observed. Single step reduction waves with well-developed limiting current

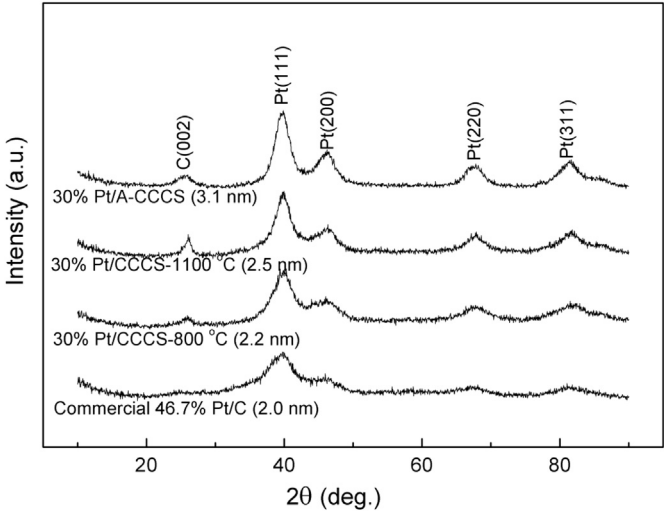


**Fig. 7.** XRD patterns of commercial 46.7% Pt/C, 30% Pt/CCCS-800 °C, 30% Pt/CCCS-1100 °C, and 30% Pt/A-CCCS catalysts.

plateaus are observed for all the catalysts. Furthermore, all the catalysts showed less than 2% hydrogen peroxide production during ORR. The ECSA of Pt was determined by charge integration under the hydrogen desorption peaks appearing between 0 and 0.35 V, by assuming a charge of 210  $\mu\text{C cm}^{-2}$  for the electroactive Pt surface [68]. The Pt/CCCS-800 °C, Pt/CCCS-1100 °C, and Pt/A-CCCS catalysts showed ECSA values of 69, 52, and 53  $\text{m}^2 \text{g}_{\text{Pt}}^{-1}$ , respectively. It is important to notice that, when Pt concentration is increased from 5% to 30%, the synergistic effect in the kinetic region is not observed due to the strong Pt active sites for ORR in 30% Pt/CCCS-800 °C.

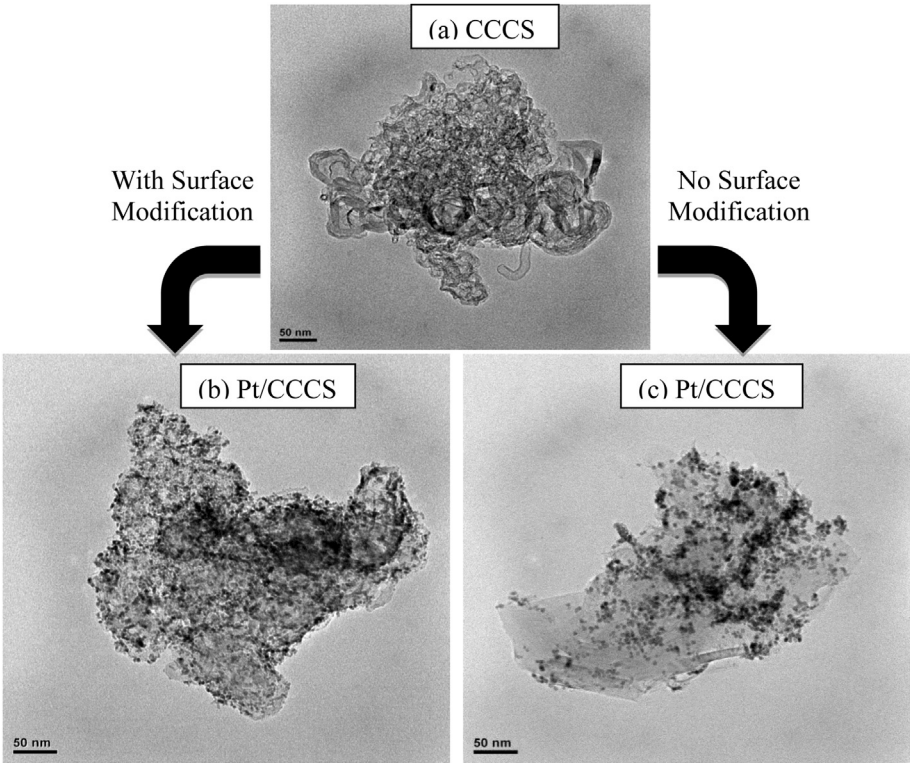


**Fig. 6.** Schematic of Pt deposition showing the effect of surface modification on the uniform distribution of Pt over the CCCS using a modified polyol process. The scale bar is 50 nm.

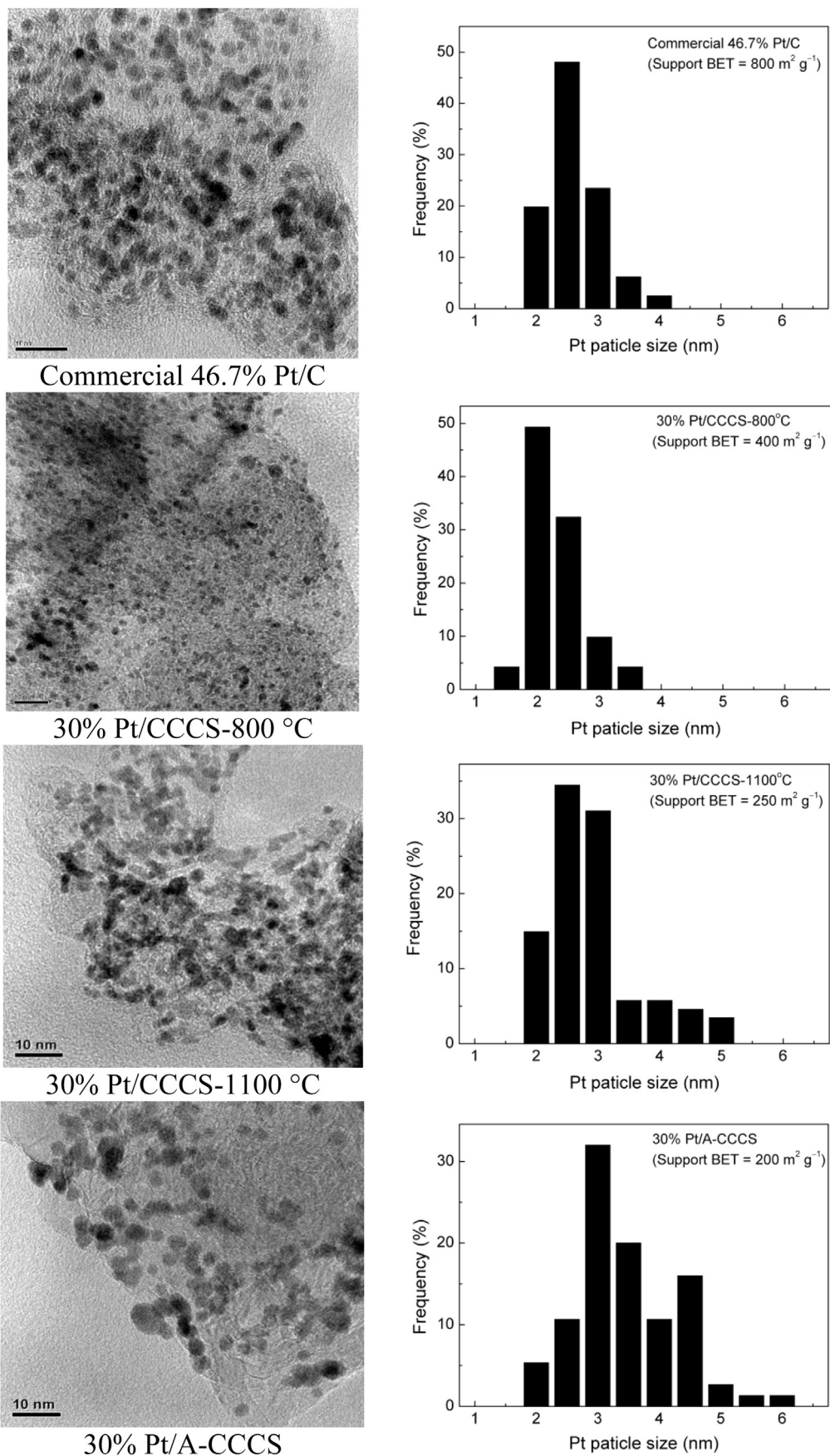


**Fig. 8.** HRTEM images and particle size distribution of commercial 46.7% Pt/C, 30% Pt/CCCS-800 °C, 30% Pt/CCCS-1100 °C, and 30% Pt/A-CCCS catalysts. The scale bar is 10 nm.

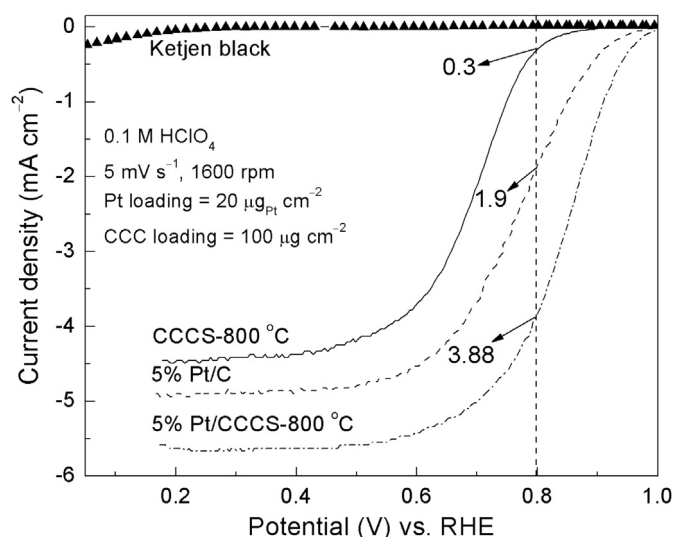


**Fig. 9.** Comparison of ORR activities of Ketjen black, CCCS-800 °C, 5% Pt/C and 5% Pt/CCCS-800 °C catalysts in rotating disk electrodes.

The H<sub>2</sub>-air fuel cell polarization performances of the 30% Pt/CCCS-800 °C and the 30% Pt/A-CCCS catalysts are compared to that of commercial 46.7% Pt/C catalyst in Fig. 11. The Pt loading on the anode and cathode electrodes are 0.1 mg cm<sup>-2</sup> as measured by the XRF. Comparison of H<sub>2</sub>-air fuel cell performance at 0.6 V<sub>ir-free</sub> showed current density values of 1600, 1350, and 1260 mA cm<sup>-2</sup> for the 30% Pt/A-CCCS, 30% Pt/CCCS-800 °C, and commercial 46.7% Pt/C catalysts, respectively. The power densities (rated) are 0.18 and 0.23 g<sub>Pt</sub> kW<sup>-1</sup> for the 30% Pt/A-CCCS and 30% Pt/CCCS-800 °C catalysts, respectively and 0.25 g<sub>Pt</sub> kW<sup>-1</sup> for the commercial 46.7% Pt/C. At very high current densities, the better fuel cell performance of Pt/A-CCCS is attributed to the stabilization process used for synthesizing the A-CCCS with optimum pore-size distribution and BET surface area which are favorable for uniform Pt deposition and Pt particle size distribution.

### 3.6. Support stability studies

Corrosion of high surface area carbon in the presence of Pt is inevitable at high potentials under PEM fuel cell operating conditions such as high oxygen concentration, high water content, and low pH which favor carbon oxidation [12,79]. During operation, the cathodes of automotive fuel cells often experience very high potentials due to startup/shutdown cycles or due to local fuel starvation at the anode [16,17,78]. Reiser et al. [17] have shown that the cathode interfacial potential difference can reach as high as 1.5 V due to the H<sub>2</sub>/air front in the anode compartment during shutdown/startup. Carbon corrosion occurs at 0.207 V vs. RHE; however, it is not detected during fuel cell operation due to its sluggish reaction kinetics [16]. In general, carbon corrosion is estimated by measuring the amount of CO<sub>2</sub> produced [46–49] or the corrosion current [16] at high applied potentials in a PEM fuel cell by supplying pure H<sub>2</sub> to the anode and pure N<sub>2</sub> to the cathode. However, the measured current is always coupled with the H<sub>2</sub>-oxidation current at the cathode due to H<sub>2</sub> cross-over from the anode through the Nafion<sup>®</sup> membrane [16]. In the present investigation, the cathode is subjected to 1.2 V constant potential for 400 h to study the support stability by measuring H<sub>2</sub>-air polarization performance at regular intervals. The cell potential loss at 800 mA cm<sup>-2</sup> current density is used as a metric to evaluate the support stability in commercial Pt/C, Pt/CCCS-800 °C, Pt/CCCS-1100 °C, and Pt/A-CCCS catalysts.

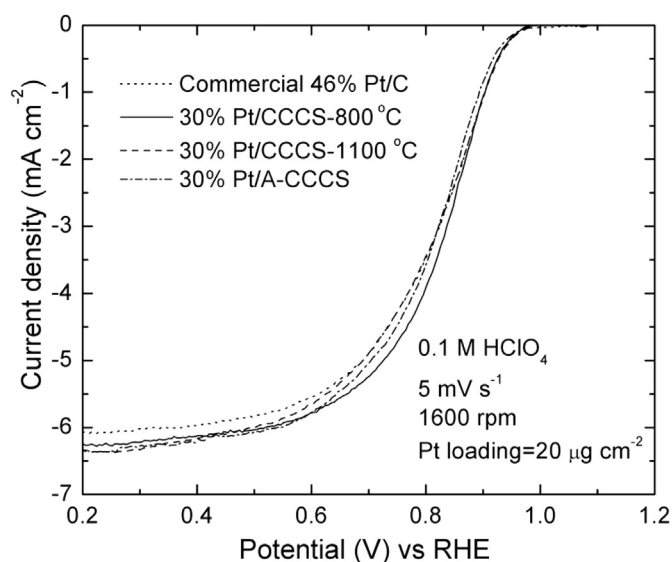


**Fig. 10.** Comparison of ORR activities of 30% Pt/CCCS-800 °C, 30% Pt/CCCS-1100 °C, and 30% Pt/A-CCCS catalysts in rotating disk electrode.

The H<sub>2</sub>-air polarization curves (initial and after 400 h) of commercial 46.7% Pt/C, 30% Pt/CCCS-800 °C, and 30% Pt/CCCS-1100 °C catalysts are compared in Fig. 12(a), Fig. 12(b), and Fig. 12(c), respectively. The commercial 46.7% Pt/C catalyst studied in this investigation is deposited on Ketjen black support which has a surface area of 800 m<sup>2</sup> g<sup>-1</sup> [73]. A very high potential loss (696 mV loss after 400 h) for the commercial Pt/C catalyst shown in Fig. 12(a) together with high mass activity loss (72%), ECSA loss (71%), and peak power density loss (85%) shown in Table 4 confirm the fact that high surface area carbon is prone to electrochemical oxidation when subjected to 1.2 V constant potential for 400 h. The commercial catalyst showed very high performance loss under mass transfer controlled region due to severe carbon corrosion at high potentials which resulted in Pt particle detachment from the support that is no longer electrochemically active, and in particle agglomeration [12]. Similar studies by Makharia et al. [16] for a 50% Pt/C indicated 30 mV loss at 1500 mA cm<sup>-2</sup> after 20 h of operation and drastic performance degradation after 30 h due to the onset of mass-transport losses induced by carbon corrosion. Electrochemical carbon corrosion is one of the most important issues that affect the long-term stability of PEM fuel cells.

Fig. 12(b) shows the initial and final (after 400 h) H<sub>2</sub>-air fuel cell polarization curves for the Pt/CCCS-800 °C catalyst subjected to a potential holding experiment for 400 h. The performance decay is evaluated by comparing the cell potential loss at 800 mA cm<sup>-2</sup>. At the beginning of the test, the Pt/CCCS-800 °C catalyst showed an i<sub>r-free</sub> cell voltage of 699 mV at 800 mA cm<sup>-2</sup> which decreased to 498 mV after 400 h potential holding at 1.2 V resulting in total cell potential loss of 201 mV. The mass activity and ECSA losses after 400 h testing are 50% and 60%, respectively with a peak power density loss of 54% (Table 4). The high cell potential loss is due to the corrosion of relatively high surface area for the CCCS-800 °C (400 m<sup>2</sup> g<sup>-1</sup>) at high potentials. The high cell potential loss for the Pt/CCCS-800 °C catalyst may be attributed to the oxidation of non-graphitic carbon initiated by the surface defects on the partially graphitized CCCS-800 °C. The C(002) peak for CCCS-800 °C in Fig. 2(a) is broader than the CCCS-1100 °C indicating the presence of amorphous and partially graphitized carbons which is confirmed by the Raman spectroscopy results shown in Table 1. Due to the heterogeneous nature of the CCCS-800 °C and the method used for the synthesis, we assume that the primary particles exhibit high

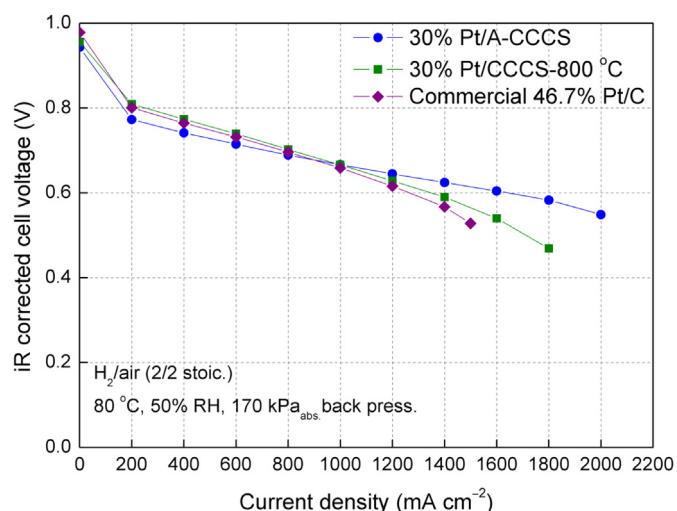


**Fig. 11.** Comparison of H<sub>2</sub>-air polarization performances of 30% Pt/CCCS-800 °C, 30% Pt/A-CCCS and commercial 46.7% Pt/C catalysts.

density of surface defects [79]. The edges of these defect sites and corners of basal planes present in CCCS-800 °C are susceptible to electrochemical oxidation and the presence of Pt can propagate the carbon corrosion under 1.2 V potential holding experiment.

The degree of graphitization of the CCCS was increased by increasing the heat treatment temperature to 1100 °C. The high temperature heat treatment resulted in a high degree of graphitization, as shown in Fig. 2(a) and Table 1, with significant decrease in the BET surface area (250 m<sup>2</sup> g<sup>-1</sup>). Platinum nanoparticles with an average d<sub>Pt</sub> of 2.5 nm were successfully deposited after the surface modification procedure. The support stability results shown in Fig. 12(c) clearly indicate the enhancement in stability for the CCCS-1100 °C at 1.2 V potential holding experiment. At 800 mA cm<sup>-2</sup> current density, the 30% Pt/CCCS-1100 °C catalyst showed an initial potential of 671 mV and a potential of 543 mV after 400 h. The initial peak power density of this catalyst is calculated to be 738 mW cm<sup>-2</sup>. The support stability test results indicated a cell potential loss of 128 mV which is much smaller than that for 30% Pt/CCCS-800 °C and commercial 46.7% Pt/C catalysts. Furthermore, the mass activity and ECSA losses are lower than that for the commercial 46.7% Pt/C and 30% Pt/CCCS-800 °C catalysts. As shown in Table 4, the mass activity loss after 400 h is 47% and the ECSA loss is only 58%. The loss in peak power density is 36%. The improved support stability is solely attributed to the high degree of graphitization of the CCCS-1100 °C. It has been reported that the extent of graphitization of carbon supports plays an important role on the support stability, with more graphitic carbons being more thermally and electrochemically stable [80–82]. However, the cell potential loss of 128 mV is significantly high for practical use in automotive PEM fuel cell stacks. Since Pt deposition is non-selective or more favorable on amorphous carbon, the CCCS-1100 °C leads to a poor stability under high potentials.

In order to further improve the support stability at high potentials, the A-CCCS was synthesized by heat treating a carbon source at 800 °C in the presence of only nitrogen-containing compound followed by a two-step stabilization process. The A-CCCS with a BET surface area of 200 m<sup>2</sup> g<sup>-1</sup> and improved hydrophobicity was used to synthesize 30% Pt/A-CCCS catalyst having an average Pt particle size of 3.1 nm.

The initial H<sub>2</sub>-air polarization curve and polarization curves obtained after 100 h, 200 h, and 400 h potential holding at 1.2 V for the 30% Pt/A-CCCS catalysts are compared in Fig. 13. The 30% Pt/A-

CCCS catalyst showed mass activity loss of 32% and ECSA loss of 30% after 400 h. Fig. 13 and Table 4 show an initial potential of 689 mV and 662 mV after 400 h potential holding with a potential loss of 27 mV. The initial peak power density is 1098 mW cm<sup>-2</sup> which

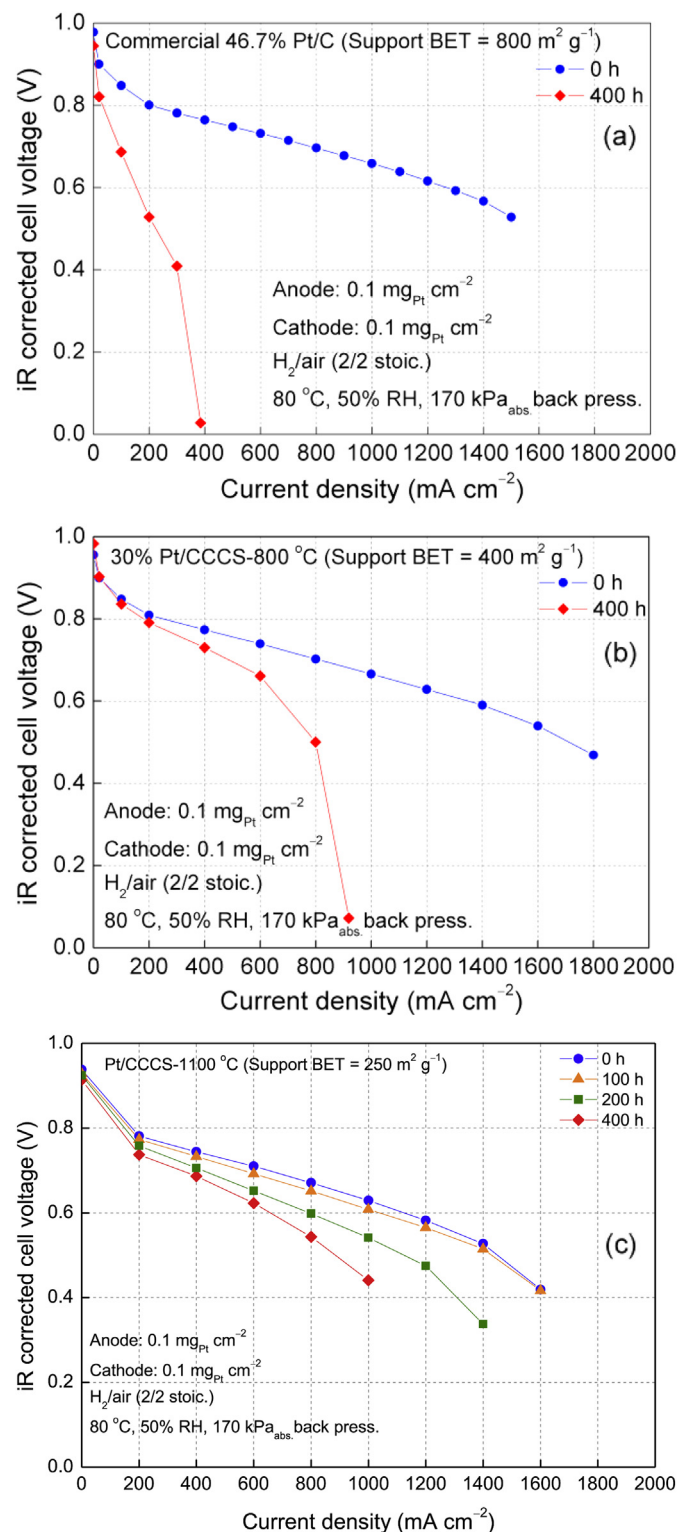


**Fig. 12.** H<sub>2</sub>-Air PEM fuel cell polarization curves of (a) commercial 46.7% Pt/C, (b) 30% Pt/CCCS-800 °C, and (c) 30% Pt/CCCS-1100 °C catalysts before and after the support stability test (1.2 V potential holding for 400 h).

**Table 4**  
Comparison of cell potential, power density, ECSA, and mass activity losses of 30% Pt/CCCS-800 °C, 30% Pt/CCCS-1100 °C, 30% Pt/A-CCCS, and commercial 46.7% Pt/C catalysts after subjecting to 1.2 V potential holding experiment.

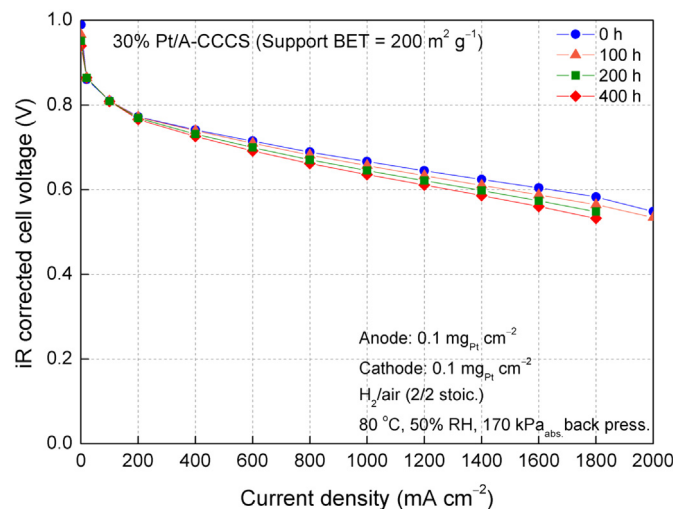
Sample	Cell potential (H <sub>2</sub> -air fuel cell) at 800 mA cm <sup>-2</sup> (mV <sub>iR-free</sub> )			Maximum power density (mW cm <sup>-2</sup> )			ECSA (m <sup>2</sup> g <sub>Pt</sub> <sup>-1</sup> )			Mass activity loss at 0.9 V <sub>iR-free</sub> (%)
	0 h	400 h	Loss (mV)	0 h	400 h	Loss (%)	0 h	400 h	Loss (%)	
Commercial Pt/C	696	0	696	794	123	85	52	15	71	72
30% Pt/CCCS-800 °C	699	498	201	863	400	54	48	19	60	50
30% Pt/CCCS-1100 °C	671	543	128	738	432	36	45	19	58	47
30% Pt/A-CCCS	689	662	27	1098	958	13	40	28	30	32

decreased to 958 mW cm<sup>-2</sup> after 400 h stability tests corresponding to a loss of only 13%.

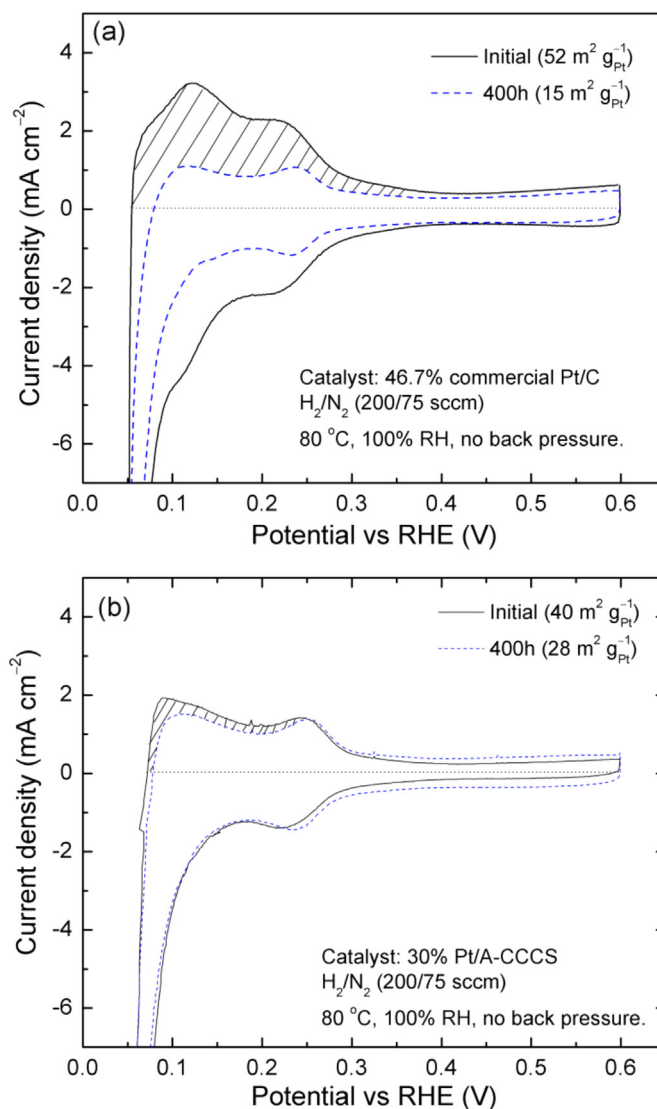
Fig. 14(a) and (b) compare the ECSA loss in the fuel cell for the commercial 46.7% Pt/C and 30% Pt/A-CCCS catalysts, respectively. The commercial Pt/C showed an initial ECSA of 52 m<sup>2</sup> g<sub>Pt</sub><sup>-1</sup> which drastically decreased to 15 m<sup>2</sup> g<sub>Pt</sub><sup>-1</sup> (71% loss) after 400 h due to severe carbon corrosion. In contrast, the 30% Pt/A-CCCS showed a ECSA loss of only 30% with initial and final ECSA values of 40 and 28 m<sup>2</sup> g<sub>Pt</sub><sup>-1</sup>, respectively.

Fig. 15(a) and (b) and Table 4 compare the electrochemical properties in a fuel cell (initially and after 400 h) including potential loss at 800 mA cm<sup>-2</sup> in H<sub>2</sub>-air, ECSA loss and mass activity loss at 0.9 V<sub>iR-free</sub> for 30% Pt/CCCS-800 °C, 30% Pt/CCCS-1100 °C, 30% Pt/A-CCCS, and commercial 46.7% Pt/C catalysts. All the fuel cell polarization results together with kinetic activity loss and ECSA loss data clearly indicate that graphitic carbon-support offers better resistance to corrosion during potential holding. Furthermore, significantly low potential loss of 27 mV at 800 mA cm<sup>-2</sup> after 400 h potential holding experiment obtained for the 30% Pt/A-CCCS catalyst is also attributed to the increased hydrophobicity of the support [46] and a relatively stronger catalyst–support interaction [50] when compared to other Pt catalysts investigated in this study. The present study shows that the graphitic structure increases the support stability when compared to the high surface area carbon support used in the commercial Pt/C catalyst. Besides the fact that the A-CCCS shows less graphitic structure in both XRD and Raman spectrum, it is more hydrophobic in nature than the CCCS-800 °C and CCCS-1100 °C as shown in Fig. 16. The hydrophobicity is one of the factors that influence the support stability. The CCCS precursor

(Ketjen black) disperses uniformly in water. As the heat-treatment temperature increases, the hydrophobicity is enhanced on the CCCS. However, there are still some carbon particles remaining in the water phase which indicates the partial graphitization of the CCCS-1100 °C. On the other hand, there is no A-CCCS in the water phase, only in the hexane phase showing its strong hydrophobicity. Since carbon corrosion is accelerated in the presence of water at high potentials [47], the more hydrophobic A-CCCS is highly corrosion resistant at the PEMFC cathode operating conditions.



**Fig. 13.** H<sub>2</sub>-Air PEM fuel cell polarization curves of 30% Pt/A-CCCS cathode catalyst before and after the support stability test (1.2 V potential holding for 400 h). The H<sub>2</sub>-air polarization performances were measured under H<sub>2</sub>/air (2/2 stoic.), 80 °C, 50% RH, and 170 kPa<sub>abs</sub>.



**Fig. 14.** Comparison of ECSA loss in 25 cm<sup>2</sup> MEAs for (a) commercial 46.7% Pt/C and (b) 30% Pt/A-CCCS catalysts.

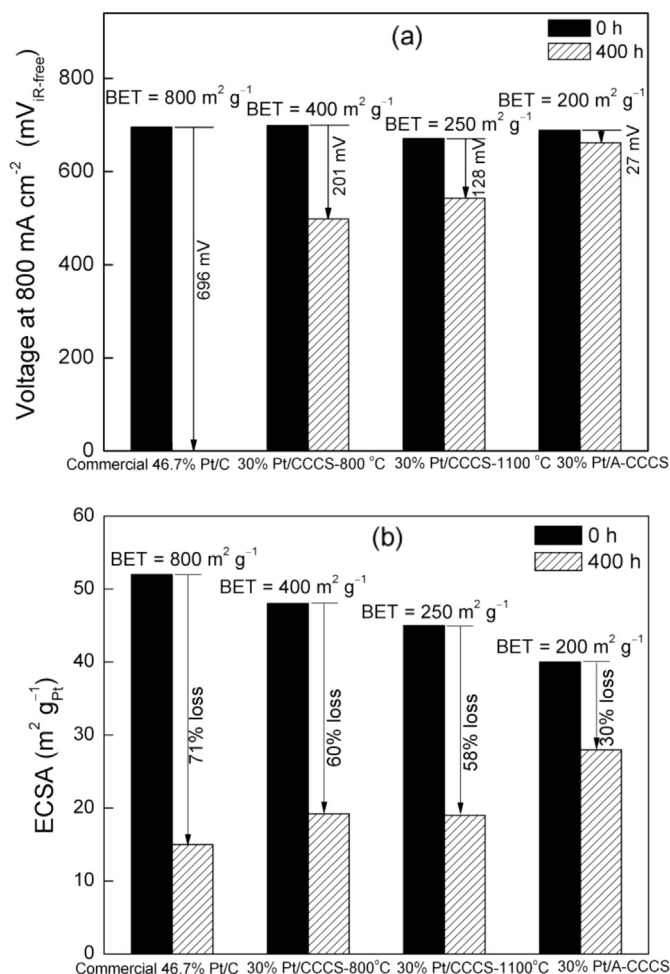


Fig. 15. Comparison of (a) cell potential losses and (b) ECSA losses of commercial 46.7% Pt/C, 30% Pt/CCCS-800 °C, 30% Pt/CCCS-1100 °C, and 30% Pt/A-CCCS catalysts after potential holding at 1.2 V for 400 h.

With the enhanced support stability for the 30% Pt/A-CCCS, we anticipate better catalyst stability when subjected to potential cycling conditions between 0.6 and 1.0 V where the Pt and Pt-based catalysts suffer loss of activity due to various processes including

metal dissolution, loss in Pt electrochemical surface area etc. Since the support is very stable at high potential, any contribution from the support degradation during catalyst durability evaluation under potential cycling conditions (0.6–1.0 V) can be eliminated.

#### 4. Conclusion

A multi-step process was developed for the synthesis of catalytically active and highly stable carbon composite catalyst supports (CCCS-800 °C and CCCS-1100 °C) and an activated carbon composite catalyst support (A-CCCS). CCCS-800 °C showed excellent activity for ORR with well-defined kinetic and mass transfer regions in RRDE studies. A stable A-CCCS was prepared for the synthesis of 30% Pt/A-CCCS catalyst. Performance evaluation studies in 25  $\text{cm}^2$  PEM fuel cell showed power densities (rated) of 0.18 and 0.23  $\text{g}_{\text{Pt}} \text{ kW}^{-1}$  for the 30% Pt/A-CCCS and 30% Pt/CCCS-800 °C catalysts, respectively. The 30% Pt/A-CCCS catalyst showed only 27 mV cell potential loss in  $\text{H}_2$ -air fuel cell polarization performance, 30% ECSA loss, and 32% mass activity loss after 400 h potential holding at 1.2 V. The enhanced support stability of 30% Pt/A-CCCS catalyst is attributed to the increased hydrophobicity and better catalyst–support interaction when compared to the commercially used high surface area carbon supports. Due to its enhanced stability at high potentials, the A-CCCS should be considered as a potential candidate for automotive PEM fuel cells.

#### Acknowledgment

The financial support of US Department of Energy (Grant no. DE-EE0000460) is gratefully acknowledged.

#### References

- [1] R. Borup, J. Meyers, B. Pivovar, Y.S. Kim, R. Mukundan, N. Garland, D. Myers, M. Wilson, F. Garzon, D. Wood, P. Zelenay, K. More, K. Stroh, T. Zawodzinski, J. Boncella, J.E. McGrath, M. Inaba, K. Miyatake, M. Hori, K. Ota, Z. Ogumi, S. Miyata, A. Nishikata, Z. Siroma, Y. Uchimoto, K. Yasuda, K. Kimijima, N. Iwashita, *Chem. Rev.* 107 (2007) 3904–3951.
- [2] W. Lubitz, W. Tumas, *Chem. Rev.* 107 (2007) 3900–3903.
- [3] H.A. Gasteiger, S.S. Kocha, B. Sompalli, F.T. Wagner, *Appl. Catal. B Environ.* 56 (2005) 9–35.
- [4] S.Y. Huang, S.M. Chang, C.T. Yeh, *J. Phys. Chem. B* 110 (2006) 234–239.
- [5] B.N. Popov, X. Li, G. Liu, J.W. Lee, *Int. J. Hydrogen Energy* 36 (2011) 1794–1802.
- [6] X. Li, H.R. Colon-Mercado, G. Wu, J.W. Lee, B.N. Popov, *Electrochem. Solid State Lett.* 10 (2007) B201–B205.
- [7] X. Li, S. Park, B.N. Popov, *J. Power Sources* 195 (2010) 445–452.
- [8] S.G. Chalk, J.F. Miller, *J. Power Sources* 159 (2006) 73–80.
- [9] M.S. Wilson, F.H. Garzon, K.E. Sickafus, S. Gottesfeld, *J. Electrochem. Soc.* 140 (1993) 2872–2877.
- [10] Y. Shao, G. Yin, Y. Gao, P. Shi, *J. Electrochem. Soc.* 153 (2006) A1093–A1097.
- [11] S.Y. Huang, P. Ganesan, S. Park, B.N. Popov, *J. Am. Chem. Soc.* 131 (2009) 13898–13899.
- [12] S.D. Knights, K.M. Colbow, J. St-Pierre, D.P. Wilkinson, *J. Power Sources* 127 (2004) 127–134.
- [13] L.M. Roen, C.H. Paik, T.D. Jarvic, *Electrochem. Solid State Lett.* 7 (2004) A19–A22.
- [14] Y.Y. Shao, G.P. Yin, J. Zhang, Y.Z. Gao, *Electrochim. Acta* 51 (2006) 5853–5857.
- [15] B. Avasarala, R. Moore, P. Haldar, *Electrochim. Acta* 55 (2010) 4765–4771.
- [16] R. Makharia, S.S. Kocha, P.T. Yu, M.A. Sweikart, W. Gu, F.T. Wagner, *H.A. Gasteiger, ECS Trans.* 1 (2006) 3–18.
- [17] C.A. Reiser, L. Bregoli, T.W. Patterson, J.S. Yi, J.D. Yang, M.L. Perry, T.D. Jarvi, *Electrochem. Solid State Lett.* 8 (2005) A273–A276.
- [18] Z. Siroma, N. Fujiwara, T. Ioroi, S. Yamazaki, K. Yasuda, Y. Miyazaki, *J. Power Sources* 126 (2004) 41–45.
- [19] M. Fowler, J.C. Amphlett, R.F. Mann, B.A. Peppley, P.R. Roberge, J. New. Mater. *Electrochem. Syst.* 5 (2002) 255–262.
- [20] E. Guilminot, A. Corcells, F. Charlot, F. Maillard, M. Chatenet, *J. Electrochem. Soc.* 154 (2007) B96–B105.
- [21] C. He, S. Desai, G. Brown, S. Bollepal, *Electrochem. Soc. Interface* 14 (2005) 41–44.
- [22] M.K. Debe, A.K. Schmoekel, S.M. Hendricks, G.D. Vernstrom, G.M. Haugen, R.T. Atanasoski, *ECS Trans.* 1 (2006) 51–66.
- [23] S.Y. Huang, P. Ganesan, B.N. Popov, *Appl. Catal. B Environ.* 96 (2010) 224–231.

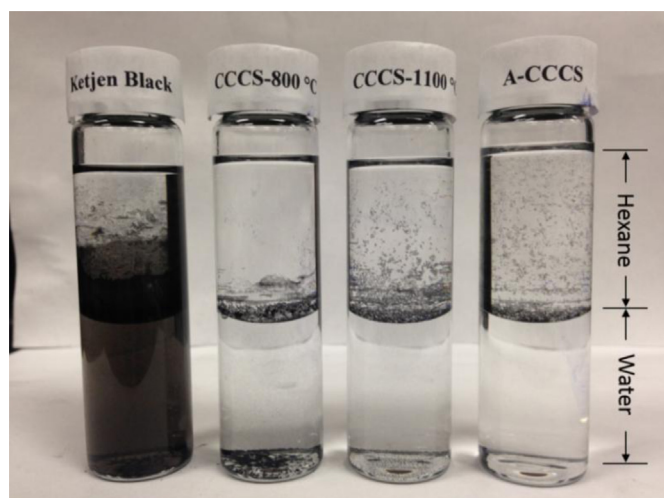


Fig. 16. Dispersions of CCCS and A-CCCS in water/hexane mixture.

- [24] P. Zhang, S.Y. Huang, B.N. Popov, J. Electrochem. Soc. 157 (2010) B1163–B1172.
- [25] S.Y. Huang, P. Ganesan, B.N. Popov, Appl. Catal. B Environ. 102 (2011) 71–77.
- [26] S.Y. Huang, P. Ganesan, B.N. Popov, ACS Catal. 2 (2012) 825–831.
- [27] S.Y. Huang, P. Ganesan, B.N. Popov, Appl. Catal. B Environ. 93 (2009) 75–81.
- [28] M.K. Debe, Nature 486 (2012) 43–51.
- [29] P.K. Sinha, W. Gu, A. Kongkanand, E. Thompson, J. Electrochem. Soc. 158 (2011) B831–B840.
- [30] D.J. Ham, J.S. Lee, Energies 2 (2009) 873–899.
- [31] B. Avsarala, P. Haldar, Int. J. Hydrogen Energy 36 (2011) 3965–3974.
- [32] H. Lv, N. Cheng, T. Peng, M. Pan, S. Mu, J. Mater. Chem. 22 (2012) 1135–1141.
- [33] H. Lv, S. Mu, Nanoscale 6 (2014) 5063–5074.
- [34] M. Wu, M. Han, M. Li, J. Zeng, S. Liao, Electrochim. Acta 139 (2014) 308–314.
- [35] R. Ornelas, A. Stassi, E. Modica, A.S. Arico, V. Antonucci, ECS Trans. 3 (2006) 633–641.
- [36] J. Wang, G. Yin, Y. Shao, S. Zhang, Z. Wang, Y. Gao, J. Power Sources 171 (2007) 331–339.
- [37] F. Xu, M. Wang, Q. Liu, H. Sun, S. Simonson, N. Ogbeifun, E.A. Stach, J. Xie, J. Electrochem. Soc. 157 (2010) B1138–B1145.
- [38] O.V. Cherstiouk, A.N. Simonov, N.S. Moseva, S.V. Cherepanova, P.A. Simonov, V.I. Zaikovskii, E.R. Savinova, Electrochim. Acta 55 (2010) 8453–8460.
- [39] G. Alvarez, F. Alcaide, O. Miguel, P.L. Cabot, M.V. Martinez-Huerta, J.L.G. Fierro, Electrochim. Acta 56 (2011) 9370–9377.
- [40] F. Forouzandeh, D.W. Banham, F. Feng, X. Li, S. Ye, V. Birss, ECS Trans. 58 (2013) 1739–1749.
- [41] D. He, Y. Jiang, H. Lv, M. Pan, S. Mu, Appl. Catal. B Environ. 132–133 (2013) 379–388.
- [42] D. He, K. Cheng, T. Peng, X. Sun, M. Pan, S. Mu, J. Mater. Chem. 22 (2012) 21298–21304.
- [43] H. Li, N. Cheng, Y. Zheng, X. Zhang, H. Lv, D. He, M. Pen, F. Kleitz, S.Z. Qiao, S. Mu, Adv. Energy Mater. 3 (2013) 1176–1179.
- [44] X. Wang, W. Li, Z. Chen, M. Waje, Y. Yan, ECS Trans. 1 (2006) 33–40.
- [45] W. Bi, T.F. Fuller, ECS Trans. 11 (2007) 1235–1246.
- [46] H.S. Oh, J.G. Oh, S. Haam, K. Arunabha, B. Roh, I. Hwang, H. Kim, Electrochem. Commun. 10 (2008) 1048–1051.
- [47] H.S. Oh, K.H. Lim, B. Roh, I. Hwang, H. Kim, Electrochim. Acta 54 (2009) 6515–6521.
- [48] K.H. Lim, H.S. Oh, H. Kim, Electrochem. Commun. 11 (2009) 1131–1134.
- [49] K.H. Lim, H.S. Oh, S.E. Jang, Y.J. Ko, H.J. Kim, H. Kim, J. Power Sources 193 (2009) 575–579.
- [50] S. Vinod Selvaganesh, G. Selvarani, P. Sridhar, S. Pitchumani, A.K. Shukla, Fuel Cells 11 (2011) 372–384.
- [51] S. Vinod Selvaganesh, P. Prishar, S. Pitchumani, A.K. Shukla, J. Electrochem. Soc. 160 (2013) F49–F59.
- [52] S. Vinod Selvaganesh, P. Sridhar, S. Pitchumani, A.K. Shukla, J. Solid State Electrochem. 18 (2014) 1291–1305.
- [53] T.K. Lee, J.H. Jung, J.B. Kim, S.H. Hur, Int. J. Hydrogen Energy 37 (2012) 17992–18000.
- [54] S.R. Dhanuskodi, M. Tam, S. Kundu, M.W. Fowler, M.D. Pritzker, J. Power Sources 240 (2013) 114–121.
- [55] K.K. Tintula, A. Jalajakshi, A.K. Sahu, S. Pitchumani, P. Sridhar, A.K. Shukla, Fuel Cells 13 (2013) 158–166.
- [56] J. Jung, B. Park, J. Kim, Nanoscale Res. Lett. 7 (2012) 34–41.
- [57] D. Spornjak, J. Fairweather, T. Rockward, R. Mukundan, R.L. Borup, ECS Trans. 41 (2011) 741–750.
- [58] A.J. Franco, M. Gerard, M. Guinard, B. Barthe, O. Lemaire, ECS Trans. 13 (2008) 35–55.
- [59] A. Pandey, Z. Yang, M. Gummalla, V.V. Atrazhev, N.Y. Kuzminyh, V.I. Sultanov, S. Burlatsky, J. Electrochem. Soc. 160 (2013) F972–F979.
- [60] N.P. Subramanian, S.P. Kumaraguru, H.R. Colon-Mercado, H. Kim, B.N. Popov, T. Black, D.A. Chen, J. Power Sources 157 (2006) 56–63.
- [61] R.A. Sidik, A.B. Anderson, N.P. Subramanian, S.P. Kumaraguru, B.N. Popov, J. Phys. Chem. B 110 (2006) 1787–1793.
- [62] V. Nallathambi, J.W. Lee, S.P. Kumaraguru, G. Wu, B.N. Popov, J. Power Sources 183 (2008) 34–42.
- [63] N.P. Subramanian, X. Li, V. Nallathambi, S.P. Kumaraguru, H. Colon-Mercado, G. Wu, J.W. Lee, B.N. Popov, J. Power Sources 188 (2009) 38–44.
- [64] G. Liu, X. Li, P. Ganesan, B.N. Popov, Appl. Catal. B Environ. 93 (2009) 156–165.
- [65] G. Liu, X. Li, P. Ganesan, B.N. Popov, Electrochim. Acta 55 (2010) 2853–2858.
- [66] X. Li, G. Liu, B.N. Popov, J. Power Sources 195 (2010) 6373–6378.
- [67] X. Li, B.N. Popov, T. Kawahara, H. Yanagi, J. Power Sources 196 (2011) 1717–1722.
- [68] H. Angerstein-Kozlowska, in: E. Yeager, J.O.M. Bockris, B.E. Conway, S. Sarangapani (Eds.), Comprehensive Treatise of Electrochemistry, vol. 9, Plenum Press, New York, 1984, pp. 15–59 (Chapter 2).
- [69] T.H. Hyeon, S.J. Han, Y.E. Sung, K.W. Park, Y.W. Kim, Angew. Chem. Int. Ed. 42 (2003) 4352–4356.
- [70] Y.A. Zhu, Z.J. Sui, T.J. Zhao, Y.C. Dai, Z.M. Cheng, W.K. Yuan, Carbon 43 (2005) 1694–1699.
- [71] J. Schwan, S. Ulrich, V. Batori, H. Ehrhardt, A. Appl. Phys. 80 (1996) 440–447.
- [72] F.C. Tai, S.C. Lee, C.H. Wei, S.L. Tyan, Mater. Trans. 47 (2006) 1847–1852.
- [73] V.A. Sethuraman, J.W. Weidner, A.T. Haug, M. Pemberton, L.V. Protsailo, Electrochim. Acta 54 (2009) 5571–5582.
- [74] X.G. Li, C.P. Liu, W. Xing, T.H. Lu, J. Power Sources 193 (2009) 470–476.
- [75] V. Stamenkovic, B.N. Grgur, P.N. Ross, N.M. Markovic, J. Electrochem. Soc. 152 (2005) A277–A282.
- [76] S. Maldonado, K.J. Stevenson, J. Phys. Chem. B 109 (2005) 4707–4716.
- [77] A.J. Bard, L.R. Faulkner, Electrochemical Methods: Fundamentals and Applications, second ed., John Wiley & Sons, New York, 2001 (Chapters 3 and 9).
- [78] A. Taniguchi, T. Skita, K. Yasuda, Y. Miyazaki, J. Power Sources 130 (2004) 42–49.
- [79] K.H. Kanagasniemi, D.A. Condit, T.D. Jarvi, J. Electrochem. Soc. 151 (2004) E125–E132.
- [80] D.A. Stevens, M.T. Hicks, G.M. Haugen, J.R. Dahn, J. Electrochem. Soc. 152 (2005) A2309–A2315.
- [81] B.J. Eastwood, P.A. Christensen, R.D. Armstrong, N.R. Bates, J. Solid State Electrochem. 3 (1999) 179–186.
- [82] Y. Shao, G. Yin, Y. Gao, J. Power Sources 171 (2007) 558–566.